Thus, the molecular g-factors for $N^{14}N^{14}O$ and for $N^{15}N^{14}O$ are essentially equal within the limits of experimental error.

VIII. CONCLUSION

The Paschen-Back effect for NH_3 and N_2O molecules has been shown to exist in the microwave spectra with only moderately strong magnetic fields. For both one- and two-nuclear couplings, the experimental results can be satisfactorily interpreted in terms of the quantum mechanical theory of perturbations.

The Paschen-Back effect in the microwave molecular spectra should prove to be useful in interpreting the nature of the spin-rotation coupling and in the direct determination of molecular g-factors.

PHYSICAL REVIEW VOLUME 76, NUMBER 10 NOVEMBER 15, 1949

Impulse Breakdown in the 10^{-9}-Sec. Range of Air at Atmospheric Pressure*,**

R. C. FLETCHER***
Laboratory for Insulation Research, Massachusetts Institute of Technology, Cambridge, Massachusetts
(Received August 1, 1949)

The formative lag of spark breakdown has been measured over the range from 0.5 to 50×10^{-9} sec. using transmission line circuits in conjunction with the micro-oscillograph. It is found to be a function only of the applied field (independent of gap-width) for the shorter times (high fields), but to increase for decreasing gap-widths for the longer times (low fields). A calculation of the formative lag is presented which is based on the assumption that it consists mainly of the time for a single electron avalanche to build up a space-charge field comparable with the applied field. This predicts the observed formative lags within the experimental accuracy of the measurements over the entire range used. The increasing times for decreasing gap-widths for the longer times is interpreted as the transition from a single avalanche to a multiple avalanche mechanism of breakdown. The critical field where this transition takes place for a given gap-width is computed and found to predict the observed critical fields within the experimental accuracy. The good agreement between theory and experiment enables a more reliable prediction than has previously been possible of the critical gap-width above which the threshold field is determined by a single avalanche mechanism.

A sharp drop in the rate of fall of the breakdown voltage is observed for the shorter times. It is suggested that this may be a change in the mechanism of electron release from the cathode.

I. INTRODUCTION

MANY experiments have been performed to measure the formative lag time of the atmospheric spark as a function of applied voltage.[1] Unfortunately this time is so short for a slight overvoltage that oscillograph measurements have previously been impossible, and other indirect schemes have had to be used. These, although often ingenious, have still limited the measurement of the formative lag to a rather small region of applied voltage (i.e., up to about 70 percent overvoltage), where the time varies extremely rapidly with the applied voltage. However, although individual measurements of the formative lag have differed from each other by as much as a factor of five, its order of magnitude and the general shape of its variation with overvoltage have been well established. In fact, the discovery that the order of magnitude of the formative lags was so short led to the suggestion that the Townsend theory had to be either modified or rejected in explaining the breakdown of atmospheric air.[2]

Proposed theories of the atmospheric spark have attempted to predict the observed threshold field and order of magnitude of the formative time.[2,3] Largely because accurate measurements of the formative time were not available, little attempt has been made to compare quantitatively the experimental and theoretical variation of the formative time with applied voltage. Raether has made the suggestion[4] that most of the formative lag consists of the time a single electron avalanche takes to build up to the magnitude where its space-charge field is comparable with the applied field. This suggestion was based on the "streamer" mechanism of breakdown, in which secondary avalanches, initiated before and behind the head of the initial avalanche by photon absorption, build up more rapidly in the enhanced field caused by the space charge. This creates two streamers of ionization which appear to move from the head of the initial avalanche towards the anode and the cathode at a much higher velocity than the velocity of the initial avalanche. Thus the complete spark channel should be established very soon after the space-charge field of the initial avalanche becomes of the order of the applied field. Raether showed that this suggestion explains the general shape

* Sponsored by the ONR, the Army Signal Corps, and the Air Force under ONR Contract N5ori-07801.

** From a doctorate thesis in physics, Massachusetts Institute of Technology.

*** National Research Council Predoctoral Fellow.

[1] A summary is given by R. Strigel, *Elektrische Stossfestigkeit* (Verlag. Julius Springer, Berlin, 1939), p. 34.

[2] J. Slepian, Elec. World **91**, 761 (1928); J. Franck and A. von Hippel, Zeits. f. Physik **57**, 696 (1929); L. B. Loeb, Science **69**, 509 (1929).

[3] L. B. Loeb and J. M. Meek, *The Mechanism of the Electric Spark* (Stanford University Press, Stanford University, California, 1941); H. Raether, Zeits. f. Physik **112**, 464 (1939).

[4] H. Raether, Elektrotech. Zeits. **63**, 301 (1942).

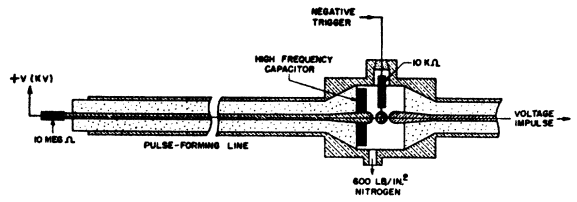

FIG. 1. Schematic sketch of u.h.s. impulse generator capable of delivering 20-kv impulses with rise times of 4×10^{-10} sec. The coaxial capacitor serves to sharpen the top of the impulse.

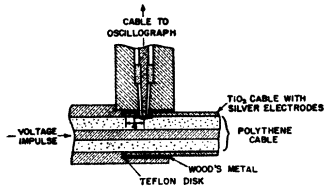

FIG. 2. Connections to u.h.s. voltage divider, consisting of two concentric coaxial transmission lines whose characteristic impedances produce a divider ratio of 100:1.

of the formative lag *vs.* overvoltage curve and the correct order of magnitude, but more exact comparison was not possible because of the limited range and accuracy of the measurements of the formative lag.

With the development of the micro-oscillograph[5] in the Laboratory for Insulation Research there arose the possibility of measuring the formative lag by oscillographic means with greater accuracy and over a wider range of times than has been previously possible. Thus, if the associated circuitry could be developed, the micro-oscillograph would be capable of measuring transients which change in times considerably less than 10^{-9} sec. Direct oscillographic measurement has the advantage that it reveals the shape of the voltage impulse being used to measure the breakdown. There is good reason to believe that many of the previous attempts to measure the formative lag were limited by oscillations or spikes on the voltage impulse and also perhaps by rise times which were too long compared to the time lags being measured.

The present investigation was conducted to measure the formative lag down to times of less than 10^{-9} sec., and to compare this measured value with a value calculated according to the suggestion of Raether. It was also thought that the oscillographic recording of the breakdown at high current levels might be of some interest.

II. EXPERIMENTAL ARRANGEMENT

In order to measure time lags down to less than one mμsec. it is necessary to have circuits capable of handling transients with frequency components in the ultra-high frequency range. These transients might justifiably be called ultra-high speed (u.h.s.) transients, and the associated circuits, ultra-high speed (u.h.s.) circuits. A brief discussion of the particular u.h.s. circuitry used in the present investigation follows, leaving a more detailed description of the required special techniques for a separate report.[5a]

Transmission lines are used as circuit connections throughout in order to eliminate the effects of stray inducatance and capacity. To generate the voltage impulse, a three-electrode trigger gap is arranged along the center conductor of a coaxial transmission line and kept under 600 p.s.i. of nitrogen (Fig. 1). The transmission line on one side of this gap is initially charged to a voltage $+V$ (of the order of 20 kv), while the other side is grounded. When the center electrode is triggered with a negative pulse the trigger gap breaks down and a voltage impulse of $V/2$ is sent down the previously grounded transmission line. A coaxial capacitor in parallel with the pulse-forming line serves to sharpen the voltage impulse. This impulse generator produces voltage impulses across the spark gap to be measured which have rise times of the order of 0.4 mμsec.

A voltage divider is required in order to view these kilovolt impulses with the micro-oscillograph. A successful design uses two concentric coaxial transmission lines, the characteristic impedances of which produce a divider ratio of 100 to 1 (Fig. 2). In order to do this the smaller impedance line is made of titanium dioxide ceramic (dielectric constant 85) while the larger impedance line is a standard 52-ohm polyethylene cable (RG17/U) (dielectric constant 2.25). Because the transition from the low to the high dielectric line excites the higher modes of the coaxial lines, the pick-off probe is placed far enough from the junction ($\frac{1}{4}$ in.) for these higher modes to be attenuated to negligible amplitudes. The ceramic line could be made conveniently only in short lengths (26 cm) so that there are reflections from the end in 16 mμsec. These reflections are confined to spikes by terminating the line with carbon resistors.

The spark gap to be tested is arranged along the center conductor of an air-dielectric coaxial transmission line with an inner conductor of 0.920 in. and an outer conductor of 2.265 in. in diameter. This is tapered to connect with the polyethylene cable so as to approximately preserve the 52-ohm characteristic impedance and still make a transition from a polyethylene to an air dielectric (Fig. 3). Circular holes are cut through the outer conductor in order to view the spark, allow for ultraviolet illumination, and permit free circulation of air. One electrode can be moved relative to the other

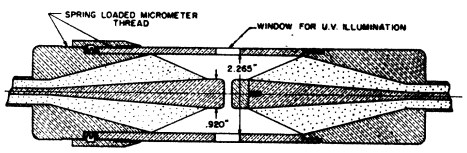

FIG. 3. Spark gap under test arranged along the center conductor of a transmission line to eliminate distortions due to stray inductance and capacity.

[5] G. M. Lee, Proc. Inst. Radio Eng. **34**, 121W (1946).
[5a] R. C. Fletcher, Rev. Sci. Inst. (to be published).

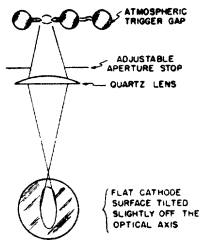

FIG. 4. Schematic sketch of ultraviolet illuminating system showing roughly the shape of illuminated area.

by means of a micrometer screw which enables the gap to be set to an accuracy of ± 0.0003 cm. The electrodes are made of brass and shaped to an approximately Rogowski profile. The faces of the electrodes are highly polished with alumina powder and then washed with acetone.

Ultraviolet illumination is provided by concentrating the light from an illuminating spark gap with an $f/2$ quartz lens on the cathode of the spark gap being tested. The illuminating gap is made the short leg of a three-electrode triggered spark gap, which is fired at least 60 mμsec. before the voltage impulse is applied across the test gap. The electrodes of the illuminating gap are pointed and the gap is made small (*ca.* $\frac{1}{8}$ in.) to cause the spark to be roughly spherical in shape and always confined to the same point in space. Although this illumination has to come from the side, by tilting the optical axis of the illuminating system slightly with respect to the plane of the electrodes, one may obtain an illumination of the center of the cathode which is roughly elliptical in shape and covers about $\frac{1}{4}$ the total area of the cathode, or about 1 cm^2, as indicated in Fig. 4. The intensity may be varied by adjusting the diameter of the aperture placed directly in front of the lens.

The spark gap is arranged in the testing circuit shown schematically in Fig. 5. Initially the two lines labeled "pulse-forming line" are charged to the voltages indicated. These serve to limit the pulses formed at the impulse generator and the illuminating gap to 75 and 150 mμsec., respectively.

The process is started by turning on the beam of the micro-oscillograph for about one millisecond by means of a mechanical switch which dips quickly in and out of a pool of mercury. A probe is inserted into the beam path, so that when the beam is first turned on, a voltage is induced on the probe, which, when amplified, fires a thyratron-ignition-coil trigger generator. The output of the ignition coil triggers the illuminating gap. This gap simultaneously begins building up a photon intensity in the spark gap, sets off a magnetron timing wave, and triggers the u.h.s. impulse generator. When the impulse generator fires, a portion of the impulse is fed into the sweep driver while the main part proceeds down a 40-ft. transmission line (RG17/U) through the voltage divider to the spark gap. Current through the spark gap is observed by feeding the other side of the gap into the oscillograph through another transmission line. The cables from the voltage divider and the spark gap are so arranged that their signals arrive at the micro-oscillograph simultaneously. Synchronization of these with the sweep was obtained by varying the length of line to the sweep driver.

The sweep circuit is a vacuum tube pentode (3D21) discharging the capacity of the deflection plate leads. It is driven by a thyratron driver (2D21). It was found that the plate of the sweep pentode began to recharge during the millisecond the oscillograph beam is turned on. To prevent this a hydrogen thyratron (3C45) discharge circuit had to be built which turns off the power supply voltage leading to the sweep pentode after the sweep has passed. This discharge circuit is triggered from the illuminating gap. Sweep speeds are obtained by this method which give full scale deflection continuously adjustable from 5 to 1000 mμsec., and which are synchronizable to ± 0.1 mμsec.

The voltage of the impulse applied across the gap is assumed to be the voltage V to which the pulse-forming line is initially charged, less 5 percent for the small part of the voltage picked off for triggering the sweep circuit. The voltage V is measured by means of the current through a 100-megohm resistor to an accuracy of ± 1 percent. Small oscillations on the top of the pulse (Fig. 7) probably decrease this accuracy for the shorter times.

III. EXPERIMENTAL RESULTS

In order to check the conditions under which later experiments were conducted, an initial measurement was made of the d.c. breakdown of air (at 760 ± 3 mm of Hg, 22 ± 1°C, and 40 ± 10 percent relative humidity), using the same voltmeter, spark gap, and general procedure as used in the later impulse measurements. The results of this d.c. measurement are plotted in Fig. 6, together with a weighted average for a number of measurements compiled by Schumann.[6]

Measurements of the impulse breakdown of air (the

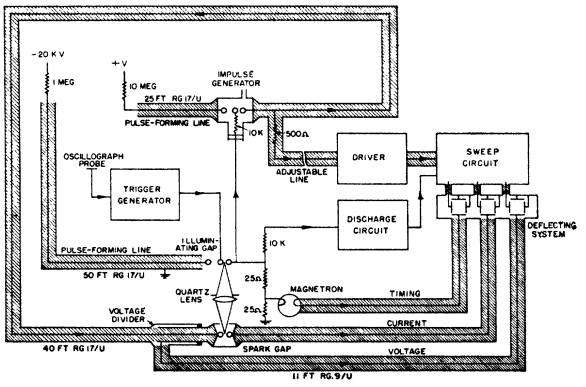

FIG. 5. Schematic diagram of u.h.s. circuit for studying impulse breakdown of air.

[6] W. O. Schumann, *Elektrische Durchbruchfeldstärke von Gasen* (Verlag. Julius Springer, Berlin, 1923), p. 26.

same conditions as for the initial measurement) were made on oscillograms obtained with the circuits described in Section II. Sketches of typical voltage traces for different conditions of applied field and gap-width are presented in Fig. 7. These sketches were prepared by tracing the image of the oscillograms formed by a micro-projector and correcting them for the effect of the known reflections in the transmission lines. It can be observed that the first evidence of breakdown after the applied voltage achieves its full size occurs at the time marked τ, which we shall define as the time lag of breakdown. The degree to which the breakdown proceeds during the rise time of the applied voltage is neglected in this definition of lag time. An estimation of the magnitude of this effect will be given later. Little additional information was obtained from the current oscillograms because of the high displacement current caused by the voltage impulse across the capacity of the spark gap.

The effect on the time lag of varying the ultraviolet illumination intensity was tested for a fixed gap-width of 1.55 mm and applied field of 82 kv/cm. For the greatest intensity used there was no detectable randomness, but as the intensity decreased the randomness increased. In Fig. 8 is plotted the logarithm of the fraction of time lags larger than τ as a function of τ. For each intensity about 35 lags were measured. It can be seen that the distribution seems to be exponential for all intensities measured, as has been found previously for longer times and lower ultraviolet intensities.[7,8] Using the experimental conclusion found by Strigel,[8] that every electron released from the cathode is successful in initiating the breakdown at this high an overvoltage (95 percent), and assuming that all of the statistical fluctuations are due to the fluctuations in the supply of initiating electrons from the cathode, we can use the observed distributions to calibrate our ultraviolet source in terms of the photoelectric current. Thus, if the distribution is $e^{-\tau/\sigma}$, $1/\sigma$ should be the rate at which electrons are released from the cathode. σ can be measured from the distribution curves to give a value of $0.0037/A^2$ mμsec., where A is the aperture diameter in inches of the ultraviolet illuminating system. This corresponds to a photoelectric current of $4.3A^2 \times 10^{-8}$ amp./cm^2.

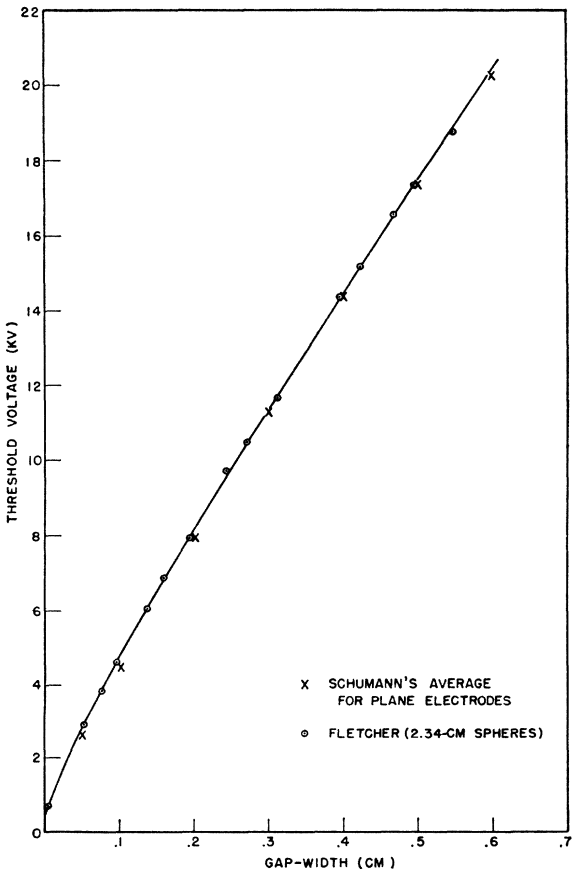

FIG. 6. D.c. threshold voltage measured under same conditions as the impulse breakdown measurements. Comparison is made with a weighted average for a number of measurements compiled by Schumann (see reference 6).

The non-statistical lag obtained for the higher intensities of ultraviolet illumination is considered the formative lag. This formative lag was measured for a variety of voltages and gap-widths for times between 0.5 and 50 mμsec. It was convenient to make runs at constant voltage rather than constant gap-width because both the adjustment of the impulse generator and the synchronization of the sweep circuit are a function of the impulse voltage. The results are plotted in Fig. 9 as a function of the applied field. For fields above 50 kv/cm the formative lag is a function of field alone independent of gap-width, while below 50 kv/cm the formative lag depends on the gap-width. Thus for fields less than the critical field (49 kv/cm), the constant voltage plot for $V=7.5$ kv begins to have longer formative lags than the other two voltages measured; for $E=42$ kv/cm the plot for $V=12.7$ kv begins to have longer formative lags.

IV. CALCULATION OF THE FORMATIVE LAG

In accordance with the suggestion of Raether[4] we shall attempt to compute the critical avalanche size as a means of calculating the formative lag. We shall consider the critical magnitude of the avalanche as the size which just reduces the field inside the avalanche to zero. This is the condition for plasma formation which must eventually be true for the whole discharge channel. Secondary avalanches may be initiated in front of and behind the initial avalanche before this space-charge field is achieved, but these secondary avalanches, building up at the same rate as the primary one, will have little effect until their rate of build-up is increased by the external space-charge fields of the

[7] K. Zuber, Ann. d. Physik **76**, 231 (1925); A. Tilles, Phys. Rev. **46**, 1015 (1934).
[8] R. Strigel, Wiss. Veroff. Siemens-Konzern **11**(2), 52 (1932).

initial avalanche and until the exponential build-up of the initial avalanche is arrested by its internal field.

In order to compute the critical avalanche size let us consider the electron avalanche in more detail. In the short times with which we are here concerned the positive ions, being so much less mobile than the electrons, will remain practically where they are created. Thus the motion of the electrons entirely determines the distribution of both ions and electrons. When the avalanche first begins, the distributions are dominated mainly by the diffusion of electrons, since the densities of electrons and positive ions are small enough that the influence of the space-charge field is negligible. For this case the rate of build-up of electron and positive ion densities, n_- and n_+, are given by the following differential equations:

$$\begin{aligned} \partial n_-/\partial t &= \alpha v n_- - D\nabla^2 n_- + v(\partial n_-/\partial z), \\ dn_+/dt &= \alpha v n_-, \end{aligned} \tag{4.1}$$

where α is the first Townsend coefficient for ionization by electron impact, v is the drift velocity in the applied field E taken in the z direction, and D is the diffusion coefficient. These equations have the following exact

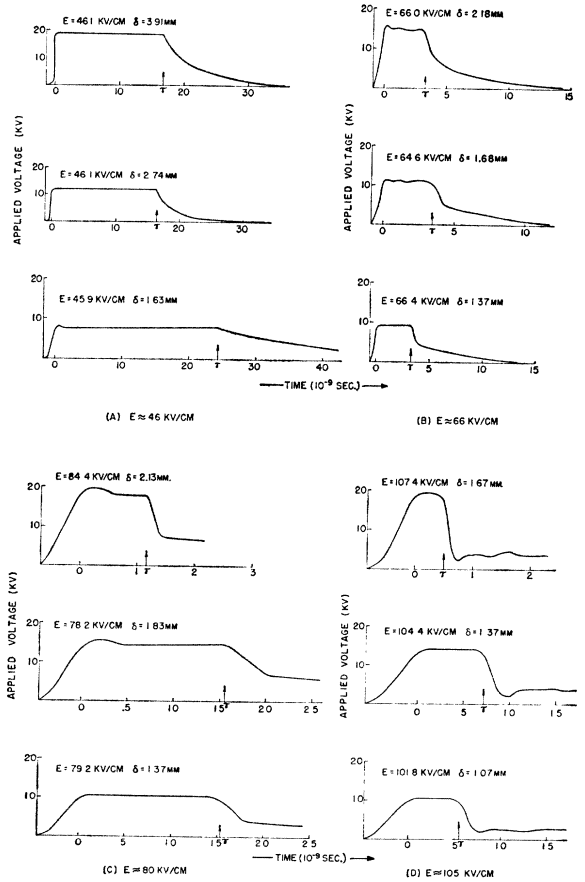

FIG. 7. Tracings of breakdown voltage for various conditions of applied field and gap-width.

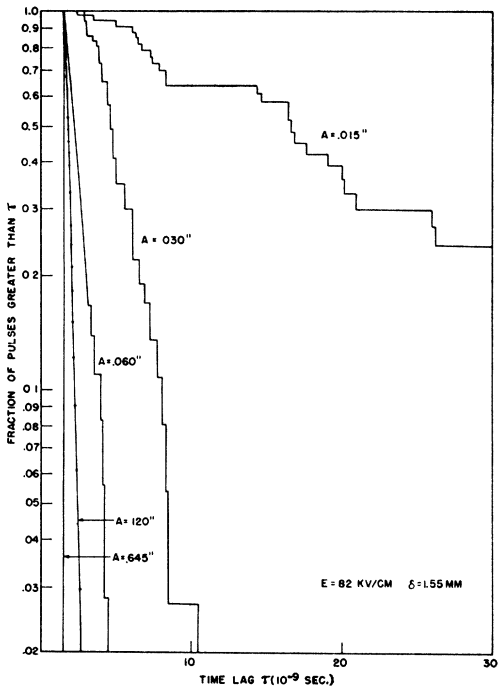

FIG. 8. Distribution of time lags for different diameter (A) aperture stops of ultraviolet illuminating system.

solutions:

$$n_- = (4\pi Dt)^{-\frac{3}{2}} \exp\left[-\frac{x^2+y^2+(z-vt)^2}{4Dt} + \alpha v t\right],$$

$$n_+ = \alpha v \int_0^t (4\pi Dt')^{-\frac{3}{2}} \exp\left[-\frac{x^2+y^2+(z-vt')^2}{4Dt'} + \alpha v t'\right] dt'. \tag{4.2}$$

It can be seen that the distribution of electrons is a normal Gaussian distribution, viewed in a coordinate system moving in the z direction with the velocity v. For this distribution the average distance of an electron from the center is well known to be $(6Dt)^{\frac{1}{2}}$, which can be considered the breadth of the avalanche.

The integral determining the positive ion distribution cannot be evaluated in terms of well-known functions. Its general behavior can be obtained by noting that the integrand is the electron distribution at the time t'. If the breadth of the avalanche at $t'=z/v$ is small compared to $1/\alpha$, the Gaussian part of the integrand will vary much more rapidly than the $e^{\alpha v t'}$. At the maximum of the Gaussian part of the integrand, $t'=z/v$, the slowly varying part can be taken in front of the integral sign, and the remaining integral can be expressed in terms of the error function

$$I(x) = \frac{2}{(\pi)^{\frac{1}{2}}} \int_0^x \exp(-x^2) dx.$$

It is convenient to introduce the characteristic length $a \equiv 4D/v$ and the distance $z_0 \equiv vt$. The length $a \equiv 4D/v$, to a first approximation, should be independent of the applied field E, since $D \sim (U_e)^{\frac{1}{2}}$ (where U_e is the average electron energy), $v \sim (E)^{\frac{1}{2}}$, and $U_e \sim E$ for the high fields considered here.[9] z_0 is the distance the center of

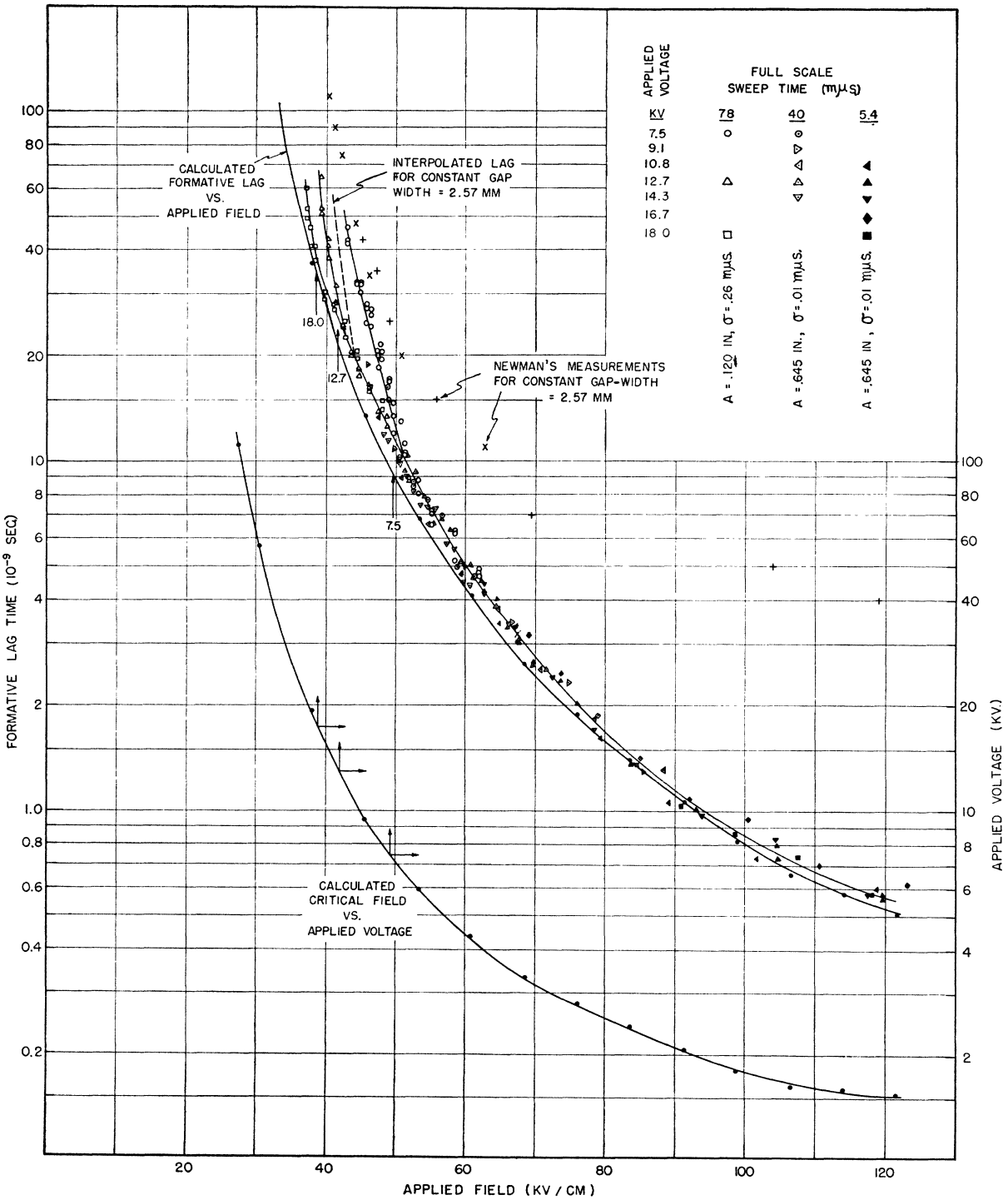

FIG. 9. Measurements of the formative lag plotted as function of applied field for different gap-widths (or applied voltages), and compared with a calculated formative lag and with the measurements of Newman (see reference 12). On the same graph are plotted the calculated critical fields, below which, for a given applied voltage, multiple avalanches (and thus longer formative lags) should be required for breakdown. The measurements are corrected for the finite rise time of applied voltage as discussed in Section V.

[9] L. B. Loeb, *Fundamental Processes of Electrical Discharge* (John Wiley and Sons, Inc., New York, 1939); A. von Engel and M. Steenbeck, *Elektrische Gasentladungen* (Verlag. Julius Springer, Berlin, 1932), Vol. I.

the electron cloud has moved. Then

$$n_-=(\pi a z_0)^{-\frac{3}{2}}\exp\left[-\frac{x^2+y^2+(z-z_0)^2}{az_0}\right]e^{\alpha z_0},$$

$$n_+=\begin{cases}\dfrac{\alpha}{2\pi az}\exp\left[-\dfrac{x^2+y^2}{az}\right]\left[1+I\left(\dfrac{z_0-z}{(az)^{\frac{1}{2}}}\right)\right]e^{\alpha z}, & z<z_0\\ \dfrac{\alpha}{2\pi az_0}\exp\left[-\dfrac{x^2+y^2}{az_0}\right]\left[1-I\left(\dfrac{z-z_0}{(az_0)^{\frac{1}{2}}}\right)\right]e^{\alpha z_0}, & z>z_0,\end{cases} \tag{4.3}$$

where the expression for n_+ is good only when the avalanche breadth $(3az_0/2)^{\frac{1}{2}}$ is small compared to $1/\alpha$.

In order to compare the two expressions for n_- and n_+, the densities can be plotted along the axis of the avalanche ($x=y=0$). It is convenient to do this in dimensionless coordinates, by plotting the densities in terms of the maximum electron density $n_0=(\pi az_0)^{-\frac{3}{2}}e^{\alpha z_0}$, and the distances in terms of $(az_0)^{\frac{1}{2}}$, which is approximately the avalanche breadth. Thus, if $w\equiv(z-z_0)/(az_0)^{\frac{1}{2}}$ and $b=\alpha(az_0)^{\frac{1}{2}}$, in the vicinity of the avalanche head ($z\simeq z_0$), Eqs. (4.3) become

$$n_-=n_0e^{-w^2},$$
$$n_+=\begin{cases}\frac{1}{2}bn_0[1+I(-w)]e^{bw}, & w<0\\ \frac{1}{2}bn_0[1-I(w)], & w>0.\end{cases} \tag{4.3a}$$

These equations are plotted in Fig. 10 for different values of the parameter $b=\alpha(az_0)^{\frac{1}{2}}$, which is approximately the ratio of the avalanche breadth to the ionizing distance $1/\alpha$. At the highest values of $\alpha(az)^{\frac{1}{2}}$ the approximation made in evaluating the integral of Eq. (4.2) is no longer good, but the general features of the curves should be correct. As $\alpha(az_0)^{\frac{1}{2}}$ increases, the cloud of electrons tends to overlap more and more the cloud of positive ions. Thus the center of mass of the electron cloud is at $z=z_0$, and its spread $(\langle x^2+y^2+(z-z_0)^2\rangle_{Av})^{\frac{1}{2}}$ is $(3az_0/2)^{\frac{1}{2}}$. The center of mass of the positive ions is approximately at $z=1/\alpha$, while its spread is $(3az_0/2)^{\frac{1}{2}}$ for $\alpha(az_0)^{\frac{1}{2}}>1$ and $\simeq 1/\alpha$ for $\alpha(az_0)^{\frac{1}{2}}<1$.

As the densities of electrons and positive ions increase due to ionization, the space charge develops a field E_s, which changes the distribution calculated above. The rate-of-build-up equation then becomes too complicated to solve exactly, and an approximation method has to be used. The simplest approximation would be to assume that the distribution is unaffected by the space-charge field. The critical avalanche size N_c could then be obtained by calculating the internal space-charge field from this distribution, and setting it equal to the applied field.

A somewhat better approximation can be obtained by the following scheme: Assume the distribution is unaffected by the space-charge field up to the time t_t at which the space charge first becomes important. At this time the space-charge field E_t can be computed from the diffusion-dominated distribution found above. For times larger than t_t assume the field is proportional

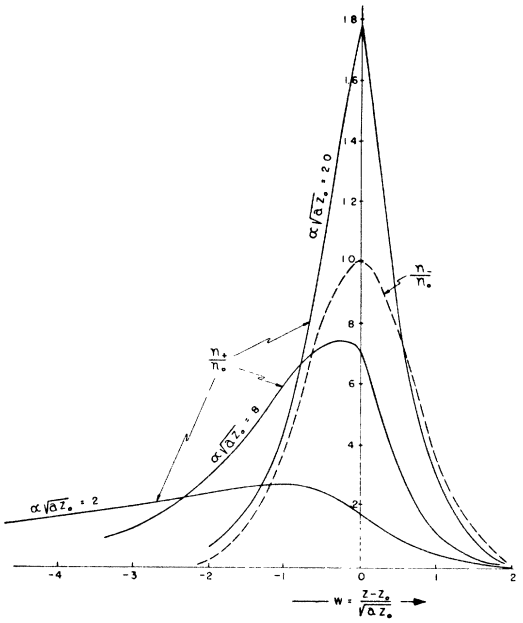

FIG. 10. Distribution of electron and positive ion densities along the axis of the electron avalanche for different values of the ratio of avalanche radius $(3az_0/2)^{\frac{1}{2}}$ to ionization distance $1/\alpha$. Densities are plotted in terms of the maximum electron density n_0, and distance from the center of electron cloud is plotted in terms of $(az_0)^{\frac{1}{2}}$, approximately the avalanche radius.

to the number of electrons N and inversely proportional to the square of the avalanche radius r_s, as would be true for a spherical distribution of charge; i.e., if $r_s=r_t$, $E_s=E_t$, and $N=N_t$ at $t=t_t$, then

$$E_s=E_t\frac{N}{N_t}\frac{r_t^2}{r_s^2}. \tag{4.4}$$

The radius r_s to be used in this equation can be obtained by integrating the drift velocity due to the space-charge field E_s. The calculations which follow are made according to this scheme.

The quantities r_t, E_t, and N_t can be computed from the condition that, at $t=t_t$, the drift velocity v_t due to the space-charge field becomes equal to the diffusion velocity $=-(D/n_-)\nabla' n_-$ (where the prime refers to the moving coordinate system). The diffusion velocity can be evaluated from Eq. (4.2) to give

$$v_t=r_t/2t_t, \tag{4.5}$$

where r_t can be taken as $(3avt_t/2)^{\frac{1}{2}}$. If we put $t_t=\ln N_t/\alpha v$ and assume $v\sim(E)^{\frac{1}{2}}$,[9] Eq. (4.5) yields a relation for E_t in terms of N_t:

$$E_t=\frac{3}{8}\frac{a\alpha}{\ln N_t}E. \tag{4.6}$$

A second relation between E_t and N_t can be obtained by calculating the space-charge field from the distribution given by Eq. (4.2). To do this it will be convenient

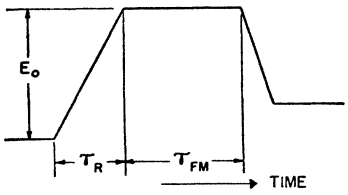

FIG. 11. Idealized shape of applied impulse.

to make several simplifying assumptions.[9a] We will assume that all the electrons are in a sphere of radius $(3az_0/2)^{\frac{1}{2}}$. This predicts fields due to the electrons which depart by a maximum of 60 percent from the fields of the actual distribution. We will further assume that the positive ions are contained in a sphere whose center is $1/\alpha$ distant from the center of the electron sphere and whose radius is $(3az_0/2)^{\frac{1}{2}}$ for $\alpha(3az_0/2)^{\frac{1}{2}}>1$ and $1/\alpha$ for $\alpha(3az_0/2)^{\frac{1}{2}}<1$ (following the analysis of Eq. (4.2) presented above). The assumption of a sphere for the distribution of positive ions for $\alpha(3az_0/2)^{\frac{1}{2}}<1$ is a poor one, but under this condition the maximum field is mainly determined by the denser electron cloud, so that a more exact knowledge of the ion distribution is not necessary. With these assumptions the equation for the space-charge field (taken at the point of maximum retarding field $z=z_0-(3az_0/2)^{\frac{1}{2}}$) is

$$E_t=\frac{e}{4\pi\epsilon_0}N_t\frac{1}{(3a/2\alpha)\ln N_t}\times\begin{cases}1+(3/2)a\alpha\ln N_t-[(3/2)a\alpha\ln N_t]^{\frac{1}{2}}, & (3/2)a\alpha\ln N_t<1\\ 1/[(3/2)a\alpha\ln N_t]^{\frac{1}{2}}, & (3/2)a\alpha\ln N_t>1\end{cases}\tag{4.7}$$

where e is the electronic charge and ϵ_0 is the dielectric constant of free space (rationalized m.k.s. units). Using Eqs. (4.6) and (4.7) to eliminate E_t, we can then obtain an implicit equation to determine N_t:

$$N_t=\frac{9\pi\epsilon_0}{4e}Ea^2\begin{cases}[1+(3/2)a\alpha\ln N_t-[(3/2)a\alpha\ln N_t]^{\frac{1}{2}}]^{-1}, & (3/2)a\alpha\ln N_t<1\\ [(3/2)a\alpha\ln N_t]^{\frac{1}{2}}, & (3/2)a\alpha\ln N_t>1.\end{cases}\tag{4.8}$$

For $N>N_t$ the avalanche radius r_s will be determined mainly by the drift velocity v_s due to the space-charge field. If we assume this velocity to be proportional to $(E_s)^{\frac{1}{2}}$,[9] r_s is given by the equation

$$r_s=r_t+\int_{t_t}^{t}v(E_s/E)^{\frac{1}{2}}dt.\tag{4.9}$$

Substituting E_s from Eq. (4.4) and differentiating, we obtain

$$r_s dr_s=v\left(\frac{E_t}{E}\right)^{\frac{1}{2}}r_t\frac{e^{\frac{1}{2}\alpha vt}}{(N_t)^{\frac{1}{2}}}dt.$$

This can be integrated to give

$$r_s^2=r_t^2+4\left(\frac{E_t}{E}\right)^{\frac{1}{2}}\frac{r_t}{\alpha}\left[\left(\frac{N}{N_t}\right)^{\frac{1}{2}}-1\right].$$

For all of the values in the region where we will use this equation, $N\gg N_t$ and $r_s\gg r_t$, so that

$$r_s^2\simeq 4\left(\frac{E_t}{E}\right)^{\frac{1}{2}}\frac{r_t}{\alpha}\left(\frac{N}{N_t}\right)^{\frac{1}{2}}.\tag{4.10}$$

The final expression for the space-charge field in terms of the avalanche size N can be obtained by the use of Eqs. (4.4), (4.6), and (4.10) to give

$$E_s=(3/16)a\alpha E(N/N_t)^{\frac{1}{2}},\tag{4.11}$$

where N_t can be computed from Eq. (4.8).

The critical avalanche size N_c, which drops the internal field of the avalanche to zero, will be attained when $E_s=E$. From Eq. (4.11) this can be seen to be

$$N_c=(256/9)N_t/(a\alpha)^2.\tag{4.12}$$

The formative lag is calculated from this by the equation

$$\tau_F=(1/\alpha v)\ln N_c.\tag{4.13}$$

In order to obtain numerical answers from these equations we will use Sanders's values[10] for α (extrapolated from lower pressures), take the value $a=3\times10^{-4}$ cm calculated from Raether's observation[11] of the avalanche breadth, and assume $v=0.224\times10^7(E)^{\frac{1}{2}}$ cm/sec., which is adjusted to the avalanche velocity observed by Raether[11] at fields near the threshold and extrapolated to the higher fields by the expected dependence on the square root of the applied field.[9] This predicts the values τ_F plotted in Fig. 9 to compare with the experimentally observed values.

V. DISCUSSION OF THE FORMATIVE LAG

Before considering how much significance should be placed on the comparison of the computed formative lag with the experimental values, let us examine the effect on the observed formative lag, as defined above, of a finite rise time of applied voltage. For simplicity let us consider a linearly rising applied field of rise time τ_R and designate the measured formative lag by τ_{FM} as shown in Fig. 11. Further, we shall assume that the ultraviolet illumination is intense enough so that the entire time lag is formative, which was the actual condition under which the experiment was conducted. With the same type of analysis used in the previous section the total time to bring about breakdown is given by the equation

$$\ln N_c=\alpha(E)v(E)\tau_{FM}+\int_0^{\tau_R}\alpha\left(E\frac{t}{\tau_R}\right)v\left(E\frac{t}{\tau_R}\right)dt.\tag{5.1}$$

[9a] Calculations using this same type of analysis were first made by Slepian, reference 2.

[10] F. H. Sanders, Phys. Rev. **44**, 1020 (1933).

[11] H. Raether, Zeits. f. Physik **107**, 91 (1937).

Since the calculated formative lag is $\tau_F=\ln N_c/\alpha(E)v(E)$, it can be expressed in terms of the measured value by the equation

$$\tau_F=\tau_{FM}+\frac{1}{\alpha(E)v(\alpha)}\int_0^{\tau_R}\alpha\left(E\frac{t}{\tau_R}\right)v\left(E\frac{t}{\tau_R}\right)dt. \quad (5.2)$$

The integral can be evaluated with the use of the empirical relations, $\alpha\sim(E-B)^2$ and $v\sim(E)^{\frac{1}{2}}$,[9] where B is a constant of the order of 24 kv. With these

$$\tau_F=\tau_{FM}+\frac{2}{7}\tau_R\frac{E^2-(14/5)BE+(7/3)B^2}{(E-B)^2}. \quad (5.3)$$

This expression was used to correct the measured points, and the corrected points are the ones plotted in Fig. 9. The correction amounted to an addition to the measured value of a practically constant value of 0.1 mμsec., which even for the smallest times amounted to only 20 percent.

The calculation of the formative lag reveals that the formative lag should be a function of field alone, independent of gap-width (or applied voltage). This is found to be true for the high fields, but not for the lower fields. For a given gap-width (or applied voltage) below a certain critical field the time lags become larger than for a larger gap-width (or smaller voltage). This critical field is believed to be the field for which the initial avalanche takes the entire gap-width to achieve the critical avalanche size. For a smaller field than this critical field a single avalanche is unable to create a high enough space-charge field to cause breakdown. More than one avalanche is required to bring about this condition. This requires the longer formative time which is observed.

To check this idea the critical field (E_c) can be computed according to the analysis of the previous section. Thus E_c should be given by the implicit equation

$$\delta=\ln N_c/\alpha(E_c) \quad \text{or} \quad V=E_c\delta=E_c\ln N_c/\alpha(E_c). \quad (5.4)$$

A plot of this calculated critical field *vs.* applied voltage is given in Fig. 9. The arrows indicate the expected critical fields for the three applied voltages used in the measurements of the longer times. The agreement with observation is well within the experimental and theoretical accuracy, confirming the validity of the interpretation of the behavior of the formative lag for the lower fields.

For the longest gap-widths used (or largest applied voltages) the observed formative lags should check the calculated values down to 39 kv/cm. It can be seen from Fig. 9 that the calculated values follow the observed values very closely, being if anything, a few percent too low. This small discrepancy is in the right direction to be explained by the neglect in the calculation of the time after the critical avalanche size has been reached until visible current is produced. However, not too much significance should be placed on the discrepancy since the velocity used in the calculation was extrapolated from a value observed by Raether to which he ascribed an accuracy of only ± 15 percent.[11] This would introduce the same percent accuracy into the calculation of the formative lag. The agreement with experiment is well within this expected accuracy.

It should be pointed out, though, that the observed agreement does not serve to distinguish between the radial space-charge field emphasized by Loeb and Meek[3] and the axial field used here. The $\ln N_c$ is insensitive to the details of the particular assumptions made in computing it. Thus a change in the value of N_c by a factor of 10 changes the calculated time lag by only 12 percent. This insensitivity was what permitted such rough assumptions made in the calculation to give good agreement with experiment. A constant value of $N_c=10^8$ would serve to predict the observed formative lag and critical field about as well as the computed variation in N_c due to the space-charge field. The main value of the computation is to establish that the correct order of magnitude for the N_c is given by considering the space-charge field of a single avalanche to be the dominating factor governing the breakdown.

In Fig. 9 comparison of the observed time lag is made with the measurements of Newman,[12] who seems to have taken the most precautions among previous workers against parasitic oscillations in his applied impulse voltage. Newman's data were taken for a gap-width the breakdown voltage of which was 10 kv, or $\delta=2.57$ mm. The broken line in Fig. 9 is interpolated from the present measurements for a constant gap-width of $\delta=2.57$ mm. Newman's measurements are about 10^{-8} sec. longer than the micro-oscillograph measurements at the same field. This could be explained by assuming that Newman defined his lag time from the bottom of his rising impulse (as seems probable from his experimental arrangement) instead of from the top as defined here, and by further assuming the rise time of his applied impulse to be of the order of 10^{-8} sec.

It is conceivable that, if the photoelectric current released by the ultraviolet illumination were too large, the experimentally determined formative lag would be decreased, making the observed agreement between computed and observed formative time lag appear as merely fortuitous. This might occur if there were a high probability of a second electron being released close to a point where the initiating electron was released, in a time small enough to influence the initial avalanche. If we assume that interaction is possible if the second electron is released a distance away from the point of release of the initial electron equal to the avalanche radius r_s, and if we further assume that interaction can occur if the second electron is released in a time $1/\alpha v$ after the first electron, the condition imposed on the

[12] M. Newman, Phys. Rev. **52**, 652 (1937).

photoelectric current is

$$(S/\pi r_s^2)\sigma \gg 1/\alpha v, \tag{5.5}$$

where S is the total illuminated area of the cathode. With the use of Eqs. (4.10), (4.6), and (4.12), the avalanche radius r_s where $N=N_c$ can be shown to be equal to $4/\alpha$, whence the condition on σ becomes

$$\sigma \gg 16\pi/S\alpha^3 v. \tag{5.6}$$

The computed value of $16\pi/S\alpha^3 v$ varies from 5×10^{-2} mμsec. at $E=38$ kv/cm, to 6.3×10^{-4} mμsec.at $E=53$ kv/cm, down to 8.5×10^{-7} mμsec. at $E=122$ kv/cm. The measurements were carried out with $\sigma=0.26$ mμsec. for $E<50$ kv/cm and $\sigma=0.01$ mμsec. for $E>50$ kv/cm. Thus the photoelectric current was on the average a factor of one hundred lower than that which would be expected to affect the formative time lag.

VI. DETERMINATION OF THE CRITICAL GAP-WIDTH

If the interpretation of the formative lag for lower fields is correct, it should be possible to predict the critical gap-width (δ_c) for which a single avalanche determines the threshold. This has been attempted previously by a number of writers,[4,13] but until recently[14] all have had to rely on a comparison of an approximate calculation of the critical field with the observed threshold field. Because of the approximate nature of the calculations, the critical gap-width has been predicted to be anywhere from 0.013 cm to 1.3 cm. With the present data it is possible to check an approximate calculation, in which, by itself, one would not have too much confidence, with two kinds of experimental observations, in which one would have considerably more confidence, to obtain a more reliable value of the critical gap-width.

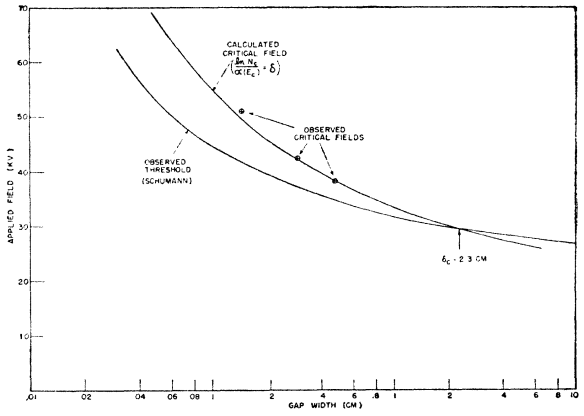

FIG. 12. Determination of the critical gap-width above which the threshold should be determined by a single avalanche.

The critical gap-width will occur when the critical field is equal to the threshold field. In Fig. 12 the calculated critical field and the observed threshold field (Schumann[6]) are plotted as a function of gap-width. The two curves are seen to cross at $\delta_c=2.3$ cm, which should be the critical gap-width.

The fact that E_c drops below E_T for $\delta>\delta_c$ indicates that it is not sufficient to drop the internal field to zero to bring about breakdown for $\delta>\delta_0$. The additional condition is that electrons must be regenerated behind the head of the avalanche. Apparently this condition requires a relatively higher field for $\delta>\delta_c$ than is required for the smaller gap-widths. This may be in part caused by the additional supply of electrons available at low gap-widths from photo-emission from the cathode which are not available at the lower gaps because of absorption in the gas. These considerations indicate that the actual δ_c may be higher than that determined from Fig. 12, and not lower as suggested by previous writers.

VII. DISCUSSION OF HIGH CURRENT DISCONTINUITY

Examination of the voltage traces of Fig. 7 reveals that for the three highest fields shown the breakdown current has a discontinuity in its rate of increase. Thus it starts out with a very rapid rate of rise and then rather suddenly changes to a slower rate of rise at a current which is of the order of magnitude of 75 amp. It is of interest to discover the cause of this discontinuity.

The first expected discontinuity in the initial electron avalanche occurs when the avalanche achieves its critical size, and the anode and cathode streamers begin. The current which is observed in the external circuit at this discontinuity should be $e.V_c v/\delta$. With the use of the calculated value of V_c the current computed from this relation is found not to exceed 10 ma over the entire range of measurements. This is much too low to account for a discontinuity of the order of 75 amp. In addition, one would expect the onset of the streamers to cause an increase in the rate of rise of current rather than a decrease.

The next discontinuities to be expected would be the arrival of either the cathode-directed or anode-directed streamers at one of the electrodes. It is difficult to estimate the current to be expected from these streamers. However, since the electrons which cause the current from the streamers have not yet reached the electrodes, the observed current should be all displacement current which should be unaffected by an insulator on either of

[13] L. B. Loeb and J. M. Meek, reference 3, p. 48; L. H. Fisher, Phys. Rev. **69**, 530 (1946).

[14] The recent measurements by L. H. Fisher and B. Bederson (Phys. Rev. **75**, 1615 (1949)) of the formative lag near the threshold offers a new method of determining δ_c. Their published data are not inconsistent with the views herein expressed if the regenerative mechanism of the modified Townsend discharge is considered to be photo-emission from the cathode and/or photo-ionization of the gas.

the electrodes. In order to test this possibility some oscillograms were taken with a disk of polystyrene first on the cathode and then on the anode. Three voltage traces, all for the same applied field, are shown in Fig. 13 to indicate the effect of an insulated electrode. It is observed that the current at the discontinuity is the same whether the insulator is on the cathode or the anode and that this current is about $\frac{1}{3}$ that observed without the insulator. This indicates that the current at the discontinuity must be at least partly conduction current. Therefore the discontinuity cannot be due to the arrival of either of the streamers at the electrodes.

A possible explanation of the discontinuity may be that a change occurs in the mode of release of electrons from the cathode. This might conceivably take place in the following way: If electron regeneration from the cathode is initially by an intense photon bombardment of the cathode with photons released by the ionization processes in the streamer, when the current builds up high enough to drop the applied field due to the generator impedance, the number of bombarding photons will drop accordingly. The field will therefore drop only to an equilibrium value for which the photoelectric current is just able to hold the field at this value. To decrease the field further another mechanism for electron release must enter. This might be by positive ion bombardment, a much slower mechanism. This would qualitatively explain the observed discontinuity. However, verification requires further experimental work.

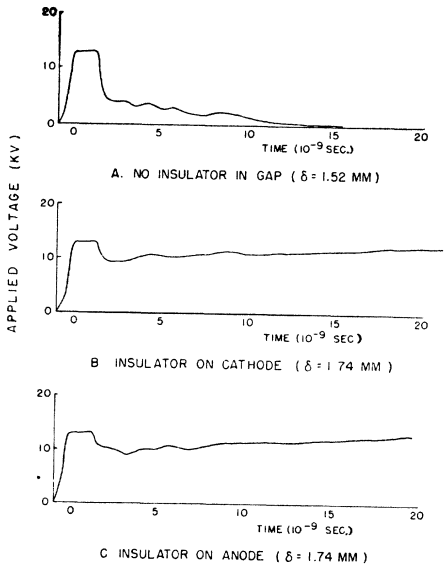

FIG. 13. Voltage traces for a spark gap with and without a 0.40-mm thick polystyrene disk, all for the same applied field (83 kv/cm).

ACKNOWLEDGMENT

The author is grateful to Professor A. von Hippel for making available to him the facilities of the Laboratory for Insulation Research and for his guidance and encouragement. He also wishes to acknowledge the constant cooperation and assistance of the members of the Laboratory.